Engineering Structures 112 (2016) 90–99

Contents lists available at ScienceDirect

Engineering Structures

journal homepage: www.elsevier.com/locate/engstruct

Flexural behavior of post-tensioned prestressed concrete girders with high-strength strands

Ho Park [a], Seungmin Jeong [b], Seong-Cheol Lee [c], Jae-Yeol Cho [d,*]

[a] Institute of Construction and Environmental Engineering, Seoul National University, Seoul, Republic of Korea
[b] Daewoo Engineering & Construction Co. Ltd., Seoul, Republic of Korea
[c] Department of NPP Engineering, KEPCO International Nuclear Graduate School, Ulsan, Republic of Korea
[d] The Department of Civil and Environmental Engineering, Seoul National University, Seoul, Republic of Korea

ARTICLE INFO

Article history:
Received 10 August 2015
Revised 23 December 2015
Accepted 2 January 2016
Available online 23 January 2016

Keywords:
High-strength strand
Post-tensioned prestressed girder
Flexural behavior
Ultimate behavior
Serviceability

ABSTRACT

Recently, high-strength strands with greater yield and tensile strength than ordinary strands have been developed in several countries. However, the influences of the high-strength strands on flexural members and code provisions have not been fully identified to date. In this study, five large post-tensioned girders were tested to investigate the effect of high-strength strands on the flexural behavior based on the concrete compressive strength and the tensile strength of the strands. The test results indicated that the actual flexural behaviors showed good agreement with the predictions of the current code, regardless of the tensile strength of the strands. The specimens exhibited ductile behavior, and the crack patterns were similar in all the specimens. Certain specimens under service load exhibited crack widths and stress in the tensile reinforcements that slightly exceeded the limit in the current codes. Because the excess was not considerable, reasonable crack control can be achieved by the proper arrangement of deformed rebars. However, further study is required to create clear guidelines.

1. Introduction

For several decades, the tensile strength of prestressing strands in prestressed concrete (PSC) members has remained at 1860 MPa, whereas concrete and reinforcing steel bars have experienced great improvements in strength. Hence, research has focused on the behavior and effect of Grade 1860 strands only [1–9]. Recently, high-strength strands with higher tensile strengths than that of conventional Grade 1860 strands have successfully been developed. Japan developed strands with tensile strengths of 2230 MPa in the early 2000s [10], and several studies in the United States investigated Grade 2069 (300 ksi) strands [11,12]. South Korea also succeeded in developing two grades of high-strength strands, 2160 MPa and 2400 MPa strands, which are increases of approximately 16% and 29% compared with that of conventional Grade 1860 strands, respectively.

With the increase in tensile strength, the yield strength has also increases, whereas other mechanical properties have remained similar to those of Grade 1860 strands. In South Korea, specifications for the mechanical properties of high-strength strands have been created in the recent revision to KS D 7002 [13]. SWPC7CL and SWPC7DL, which are the grade designations for 2160 MPa and 2400 MPa strands, have the same geometric shape, weight, and elastic modulus as those of Grade 1860 strands. Additionally, the same restrictions on the total elongation and relaxation loss are imposed for high-strength strands; the total elongation must be at least 3.5%, and the relaxation loss at 1000 h after tensioning up to 70% of the minimum breaking strength must be below 2.5% for low-relaxation strands. The tests performed by the strand manufacturer in South Korea revealed that the total elongation ranged from 6.00% to 9.48%, and the relaxation loss was between 0.90% and 1.70%.

Because of the increase in the yield and tensile strengths without loss of any other mechanical properties, high-strength strands may have several benefits in PSC members, including reducing the section size, increasing spans of structures, and reducing fabrication costs. However, because experimental results are currently too limited to verify the structural performances of PSC members with high-strength strands, it is necessary that more tests be conducted to investigate whether the current code provisions can be applied for PSC members with high-strength strands or if suitable design guidelines should be established. Therefore, in this study, an experimental program was conducted to investigate the flexural behavior of large-scale post-tensioned PSC girders with high-strength strands. The ultimate capacity and serviceability observed

* Corresponding author.
E-mail address: jycho@snu.ac.kr (J.-Y. Cho).

http://dx.doi.org/10.1016/j.engstruct.2016.01.004
0141-0296/

Nomenclature

c_2	distance from neutral axis to extreme tension fiber, mm
d	distance from extreme compression fiber to centroid of longitudinal tension rebar, mm
d_p	distance from extreme compression fiber to centroid of prestressing steel, mm
E_c	elastic modulus of concrete, MPa
e	distance from neutral axis to centroid of prestressing steel, mm
f_{ci}	compressive stress of concrete at prestressing, MPa
f'_c	specified compressive stress of concrete, MPa
f_{cr}	modulus of rupture, MPa
f_{cu}	compressive stress of concrete at test, MPa
f_{pi}	initial prestress, MPa
f_{pj}	stress in prestressing steel due to jacking force, MPa
$f_{ps,ACI}$	stress in bonded prestressing steel at nominal flexural strength, MPa
f_{pu}	nominal tensile strength of strand, MPa
$f_{pu,mea}$	measured breaking strength of strand, MPa
f_s	stress in reinforcing steel bar at service load, MPa
f_{se}	effective prestress, MPa
h	height of section, mm
I_g	moment of inertia of gross section about centroidal axis, mm^4
L	span length, mm
M_{cr}	cracking moment, kN m
$M_{cr,cal}$	theoretical cracking moment at center of specimen, kN m
M_d	moment due to self-weight at center of specimen, kN m
M_{max}	maximum moment measured during test of specimen, kN m
$M_{n,ACI}$	nominal flexural strength calculated complying with ACI 318 code at center of specimen, kN m
P_e	effective prestressing force, kN
P_i	initial prestressing force, kN
$P_{n,ACI}$	applied concentrated load corresponding to $M_{n,ACI}$, kN
r	radius of gyration of gross section, mm
t_{pre}	concrete age at prestressing, day
t_{test}	concrete age at test, day
β_1	factor relating depth of equivalent rectangular compressive stress block to neutral axis depth
γ_p	factor for type of prestressing steel
Δ_{cr}	center deflection at the first flexural cracking, mm
Δ_i	camber, mm
$\Delta_{i,cal}$	theoretical camber, mm
Δ_{max}	maximum center deflection during test of specimen, mm
Δf_{ps}	stress in prestressing steel after decompression at full service load, MPa
ρ_p	prestressing steel ratio
ω	tension rebar index
ω'	compression rebar index

through the tests were compared with several code provisions to evaluate the applicability of the code provisions for high-strength strands.

2. Experimental program

2.1. Test variables

In total, five post-tensioned PSC girders were fabricated and tested. The test variables were the compressive strength of the concrete and the tensile strength of the prestressing strands. The compressive strength of the concrete was considered as a test variable in order to investigate that higher strength of concrete provides more efficient use of high-strength strands. There was a concern that normal strength concrete would not be capable of causing the high-strength strands to yield. Two different design compressive strengths of concrete were considered: 40 MPa and 70 MPa. The former represents normal strength concrete (N-series) conventionally used for PSC girders, and the latter represents high-strength concrete (H-series). Three grades of seven-wire prestressing strands were prepared to fabricate the test specimens. The prestressing strands are referred to as SWPC7BL, SWPC7CL, and SWPC7DL, which were designated as Grade 1860, 2160, and 2400 strands, respectively. With the consideration of the test parameters, each specimen was named accordingly to represent the concrete compressive strength and strand grade, as presented in Table 1. The measured compressive strengths of the concrete and the actual tensile strength of the strands are also summarized in the table. The symbols f_{ci} and f_{cu} represent the average compressive strengths of the concrete measured at the days of prestressing t_{pre} and test t_{test}, respectively. Concretes gained the compressive strengths close to the specified values except the HC specimen. The actual tensile strengths of the strands $f_{pu,mea}$ were obtained from the results of the coupon tests performed by strand manufacturer. Typical stress–strain relationships of Grade 1860 strand and high-strength strands are plotted in Fig. 1.

2.2. Design and fabrication of the test specimens

The cross-section of the girders was designed in compliance with the Korean Highway and Bridge Design Code (KHBDC) [14], which is identical to the design methodology of ACI 318 code [15] for a flexural member. The geometry, which includes the prestressing steel ratio ρ_p of 0.195%, was initially determined based on the ND specimen and kept constant for the other specimens. The ND specimen was considered as a girder of a PSC bridge with a deck slab of 19 m wide. The geometry of the ND specimen was designed to ensure that the PSC bridge with the deck slab and the girders resisted the factored load combinations specified in the design code. In the test program, however, the deck slab was not fabricated due to the cost and time. The absence of the deck slab caused no problems with achieving the purpose of the study. The specimens exhibited sufficient flexural deformations and strengths to evaluate the code provisions regarding flexure. Near both ends of the specimens and the diaphragms, the cross-section gradually becomes rectangular to accommodate the anchorages. A girder length of 20 m was determined to minimize the effect of anchorage slip on the effective prestressing force. Details of the test specimens are illustrated in Fig. 2.

Twelve prestressing strands with a diameter of 15.2 mm were placed in each duct, and two ducts were placed with a parabolic profile. The prestressing force was applied to the specimens approximately 3 weeks after concrete placement; however, the ND specimen was prestressed 1 month after concrete placement. The strands were tensioned up to 81% of the yield strength to achieve a full prestressed condition under a full service load, and the strands in the bottom duct were tensioned before prestressing the other strands. The jacking forces were controlled by the load

Table 1
Specimen notation and the material properties of concrete and strands.

ID	f'_c (MPa)	f_{ci} (Mpa)	t_{pre} (day)	f_{cu} (Mpa)	t_{test} (day)	f_{pu} (MPa)	$f_{pu,mea}$ (MPa)	f_{pj} (MPa)	f_{pi} (MPa)	f_{pe} (MPa)
NB	40	43.3	19	42.9	30	1860	1978	1296	1150	1105
NC	40	46.2	20	46.4	30	2160	2299	1539	1377	1329
ND	40	34.3	30	39.5	51	2400	2472	1701	1528	1453
HC	70	52.8	18	50.7	27	2160	2299	1539	1377	1331
HD	70	56.1	21	69.5	34	2400	2472	1701	1528	1474

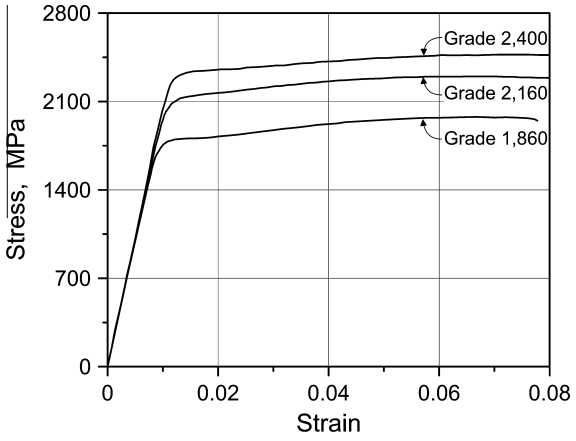

Fig. 1. Typical stress–strain relationships of Grade 1860 strand and high-strength strands.

indicator equipped in the hydraulic jack and the elongation of the strands. The jacking, initial, and effective prestress in strands were presented in Table 1.

Stirrups were placed with a spacing of 200 mm along the entire length of the specimens to prevent shear failure of the specimens. A smaller spacing of 150 mm was used at the anchorage regions. Longitudinal deformed rebars were arranged to hold the stirrups and to control crack widths. The deformed rebars used for the specimens had a nominal diameter of 12.7 mm and a nominal tensile strength of 400 MPa.

2.3. Test setup and procedure

The specimens were placed on roller supports and loaded by two separate hydraulic actuators with a capacity of 1000 kN (see Fig. 2). The actuators were symmetrically located, where each were positioned 3 m apart from the center of the specimen to provide a constant moment region of 6 m.

During the test, the applied load was measured by load cells built in the hydraulic actuators, and the vertical deflections at the center of the specimens and the two loading points were measured by draw-wire displacement transducers. To obtain the strain distribution along the depth, several electrical resistance strain gauges (ERSGs) were installed on the surface of the concrete and the longitudinal deformed rebars at different distances along the sections, which are located at the center of the specimens and the loading points for the NB, NC, and HC specimens. In the case of the ND and HD specimens, several modifications to the aforementioned ERSG schemes were made to obtain better measurements; the measuring location was shifted 1.5 m from the midspan toward both ends of the specimen to minimize the effect of the diaphragm, and the ERSGs on the concrete surface around the bottom flanges were replaced with Ω-shaped displacement transducers with a capacity of 5 mm and a gauge length of 100 mm.

To measure strains in the prestressing strands, ERSGs were attached to the strands at 1.5 m left from the midspan, though most of the ERSGs were destroyed during prestressing and grouting. Hence, LVDTs with gauge lengths of 460 mm were attached to the concrete surface at the level of the centroid of the ducts in the considered sections such that average tensile strains in the

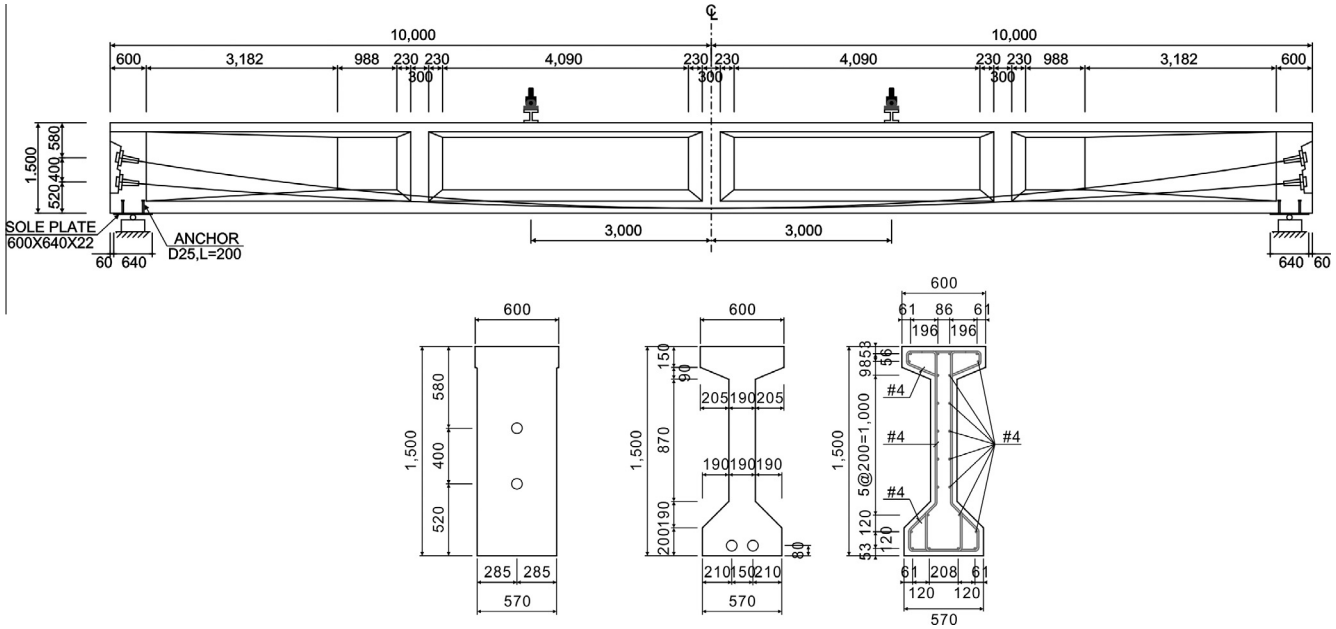

Fig. 2. Details of the test specimens and test setup.

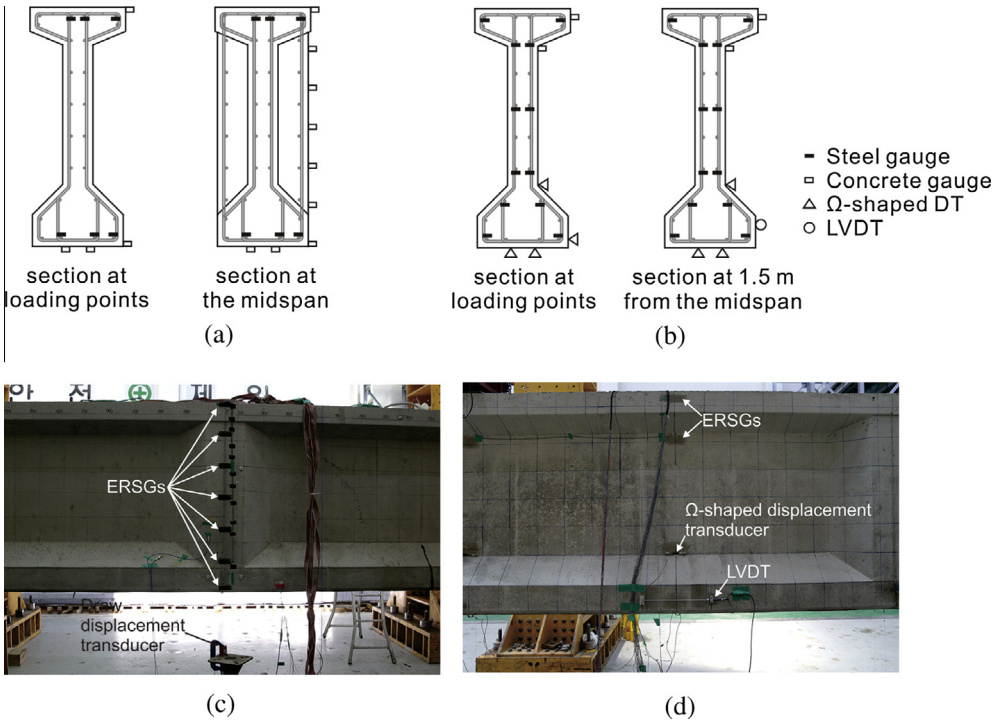

Fig. 3. Instrumentations: (a) arrangement for specimens NB, NC, and HC; (b) arrangement for specimens ND and HD; (c) photo of specimen HC at midspan; and (d) photo of specimen HD at 1.5 m from the midspan.

pure bending region could be measured. To measure the crack widths, four Ω-shaped displacement transducers were attached in the pure bending region. Fig. 3 shows the locations and photos of the instruments installed on the specimens.

The displacement-control method was used during the test, and the loading rates were varied from 0.03, 0.05, and 0.5 mm/s until reaching center deflections of 30 mm and 200 mm and the end of the test, respectively. Because of the safety concern, the test was terminated when the specimens remained in a state where the load only slightly increased when the displacement was significantly increased; from this, it was inferred that the strands yielded. The only exception was the HC specimen, which collapsed completely.

The NB, NC, and HC specimens experienced a monotonically increasing loading history until the end of the tests. However, for the ND and HD specimens, loads were removed once initial flexural cracks were observed with the naked eye. This unloading was performed to install instruments to measure the crack widths. After installing the instruments, reloading was applied until the end of the tests.

3. Experimental results

3.1. Overall responses

Load-center deflection responses for the five specimens are presented in Fig. 4. As observed, in general, all the specimens exhibited a linear response before cracking. Afterwards, the stiffness on the load-center deflection response decreased as the applied load increased; then, a plastic response was observed due to yielding of the longitudinal tension rebars until the test was finished. The difference in the load between the two actuators was measured during the test, though it was only approximately 4% of the maximum applied load at the end of the test. As mentioned earlier, all the specimens exhibited typical flexural behaviors, where there was no evidence of the effect of shear. At the end of the test, while the four specimens, with the exception of the HC specimen, did not exhibit a clear failure mode, only the HC specimen completely failed due to the concrete being crushed accompanied with buckling of the reinforcing steel bars near the loading point with the larger load value, as presented in Fig. 5(a). Although there was significant damage due to the failure, it was observed that the strands did not rupture even at the failure point, which was checked by cutting the failed section after the test, as shown in Fig. 5(b), where it can be observed that there was no damage on the strands.

The moments calculated from the applied load and center deflections are summarized in Table 2, which also includes the theoretically calculated values for comparison. The cracking moment M_{cr} is the value recorded at the time when the first crack was observed with the naked eye. The theoretical cracking moment $M_{cr,cal}$ is the value calculated at the center of the specimen using the following equation:

$$M_{cr,cal} = f_{cr} I_g / c_2 + P_e (r^2/c_2 + e) - M_d \quad (1)$$

where the modulus of rupture f_{cr} was assumed to be $0.63\sqrt{f'_c}$ and M_d was theoretically calculated to be 650 kN m. Time-dependent losses were estimated according to Eurocode 2 when calculating the effective prestressing force P_e because the time-dependent losses were not measured. The initial and effective prestress were presented in Table 1. The initial prestressing forces P_i were around 89–90% of the jacking force, with consideration of friction loss and anchorage slip, and they were verified through the measured strains in strands. Compared in the table, the calculated cracking moments slightly over-estimated the measured values. In the case of the N-series specimens, where the f_{cu} values are similar but the f_{pu} values are different, the cracking moment and the center deflection at cracking Δ_{cr} increased with the prestressing force; the ratios of the cracking moments of the NC and ND specimens to that of the

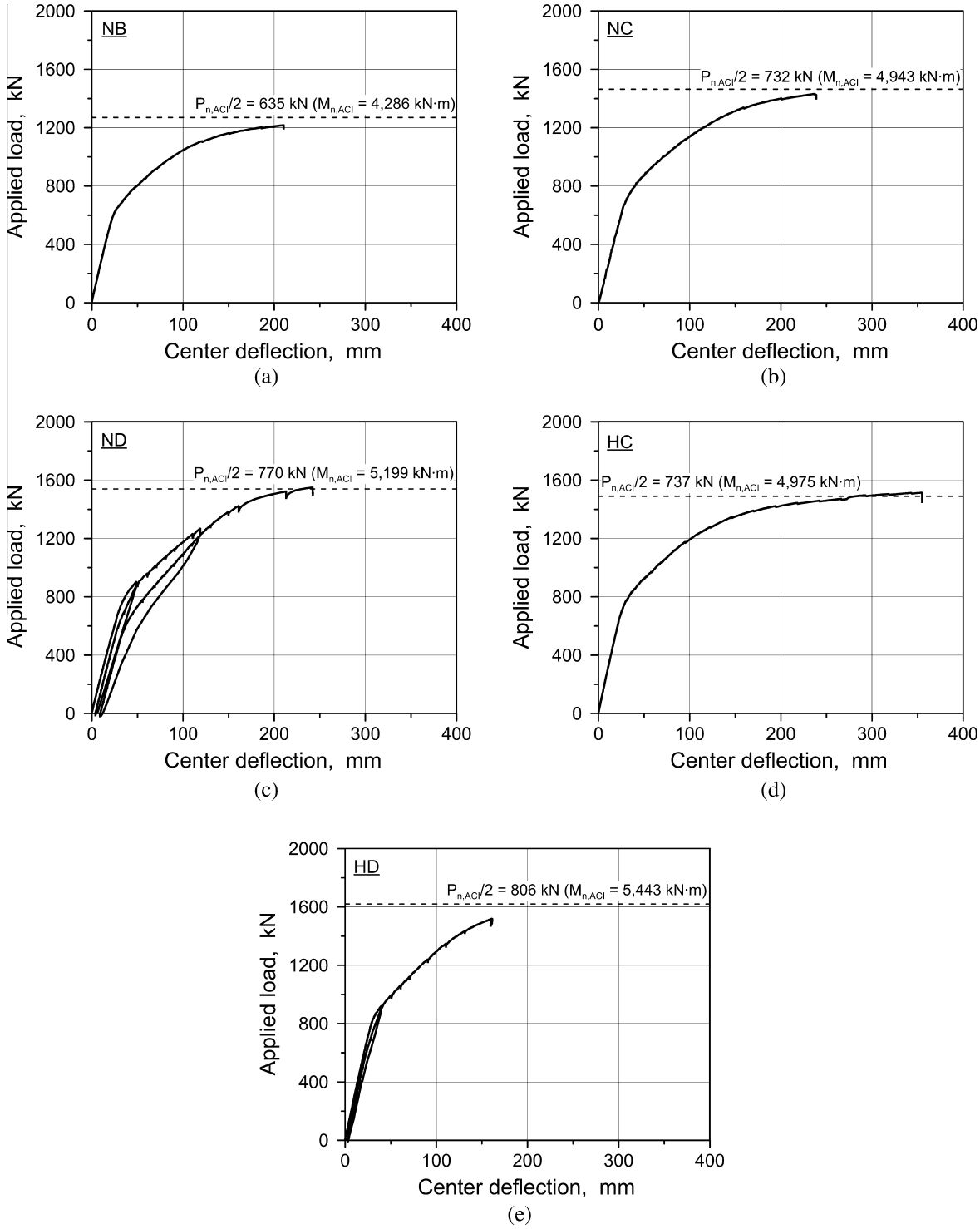

Fig. 4. Load-center deflection response: (a) NB; (b) NC; (c) ND; (d) HC; and (e) HD.

NB specimen were 1.10 and 1.22, respectively. Comparing the ND and HD specimens, where the f_{cu} values were different but the f_{pu} values were the same, cracking moment increased but center deflection at cracking slightly decreased as compressive strength of concrete increased.

The maximum moments M_{max} measured at the end of the test were compared with the nominal flexural strengths according to the ACI 318 code $M_{n,ACI}$. Note that the maximum moments M_{max} were obtained from the larger load value between the two actuators, and the nominal flexural strengths $M_{n,ACI}$ were calculated at the center of the specimens as follows:

$$M_{n,ACI} = A_p f_{ps}(d_p - a/2) \quad (2)$$

Compared in the table, the ratios of $M_{max}/M_{n,ACI}$ ranged between 1.03 and 1.09 for all the specimens except for the HD specimen. The test for the HD specimen was unintentionally stopped by an unexpected accident; it was fell down from the supports due to the lack of constraints on the transverse movement. If a comparison is made between the maximum moments and the nominal flexural strengths at the loading point, the moment ratios of all the specimens increased by approximately 0.05. Consequently, it can be said that the specimens were capable of achieving the

(a) (b)

Fig. 5. Failure of the specimen HC: (a) failure mode; and (b) strands after failure.

Table 2
Summary of test results.

ID	M_{cr} (kN m)	$M_{cr,cal}$ (kN m)	M_{cr} / $M_{cr,cal}$	M_{max} (kN m)	$M_{n,ACI}$ (kN m)	$M_{max}/M_{n,ACI}$	Δ_i (mm)	$\Delta_{i,cal}$ (mm)	$\Delta_i/\Delta_{i,cal}$	Δ_{cr} (mm)	Δ_{max} (mm)
NB	2072	1950	1.06	4429	4286	1.03	6.5	6.1	1.07	24.5	210
NC	2282	2357	0.97	5354	4943	1.08	8.8	8.3	1.06	28.7	239
ND	2531	2507	1.01	5379	5199	1.03	10.8	10.9	0.99	32.6	234
HC	2315	2395	0.97	5400	4975	1.09	8.8	8.0	1.10	24.7	355
HD	2700	2773	0.97	5221	5443	0.96	11.0	9.3	1.18	30.8	159

nominal flexural strengths. From comparison through the N-series specimens, the maximum moment increased by 17% and 26% as the tensile strength of the prestressing strands increased by 16% and 25%, respectively, which were quite close to the predictions of ACI 318 code as presented in Table 2.

The camber Δ_i measured at the center of the specimen during prestressing was compared with $\Delta_{i,cal}$, which is the theoretically calculated camber using the following equation:

$$\Delta_{i,cal} = 5(P_i e - M_d)L^2/48E_c I_g \tag{3}$$

Compared in the table, the calculated cambers agree well the measured cambers.

3.2. Crack patterns

The initial cracks occurred within the constant moment region. As the load increased, the flexural cracks grew vertically toward the upper flange and propagated from the constant moment region toward the supporting points. The overall crack patterns were similar in all of the specimens, as shown in Fig. 6. From the number of cracks within the constant moment region, the average crack spacings were evaluated, which were 164, 187, 169, 169, and 175 mm in the NB, NC, ND, HC, and HD specimens, respectively. Consequently, no relationships were found between the average crack spacing and the tensile strength of the prestressing strand, which is compatible with the average crack spacing models provided in the design codes [14,16]; the average crack spacing is affected by the rebar ratio and diameter and the bond condition and not by the tensile strength of the prestressing strand.

3.3. Load–strain relationships

Fig. 7 shows the compressive strain of the concrete and the tensile strains of the steel bars at the loading point of the HC specimen. Abrupt changes in the strains under an applied load of approximately 1000 kN occurred due to cracking at the section. Because the strain gauges were located at the loading points, which might not coincide with the first flexural crack, the strain gauges exhibited abrupt change under the load larger than the flexural cracking load in Table 2. The consistent linear responses of the concrete strain prior to the cracking changed to a curvilinear response after cracking. The steel strains increased with a steeper slope until an applied load of 1240 kN and then maintained their values as the applied load increased, which was followed by a drastic increase before the failure of the specimen.

Fig. 8 shows the strains measured at seven different locations along the depth of the section at the left loading in the ND specimen. Fig. 9 shows the strain distributions along the depth, which were evaluated from the measured strains in Fig. 8. As seen in the figure, the strain distribution along the depth is linear under the cracking load. Although the strains at the tension rebars were considerably smaller than the regression line, it can be explained with the bond mechanism between the rebars and concrete; the rebar strains have significant variation between cracks. Fig. 10 depicts the moment–curvature relationships of the ND specimen, in which the curvature was evaluated from the slope of the regression line in Fig. 9. From these figures, it can be concluded that the conventional flexural strength model based on the linear strain distribution can be applied to evaluate the ultimate flexural capacity of prestressed concrete beams with high-strength strands.

4. Comparison with design codes

4.1. Flexural strength and tension stresses at flexural failure

To calculate the nominal flexural strength of PSC members, it is essential to estimate the stress in the strand at the ultimate status. The current ACI 318 [15] provides an approximate equation to estimate the stress in the ultimate status, $f_{ps,ACI}$, as follows:

$$f_{ps,ACI} = f_{pu}\left[1 - \frac{\gamma_p}{\beta_1}\left\{\rho_p \frac{f_{pu}}{f'_c} + \frac{d}{d_p}(\omega - \omega')\right\}\right] \tag{4}$$

where f_{pu} is the nominal tensile strength of the strand, γ_p is a factor for the type of prestressing steel, β_1 is a factor that considers the depth of the equivalent rectangular compressive stress, d and d_p are the distances from the extreme compression fiber to the centroid of the longitudinal tension rebar and to the centroid of the

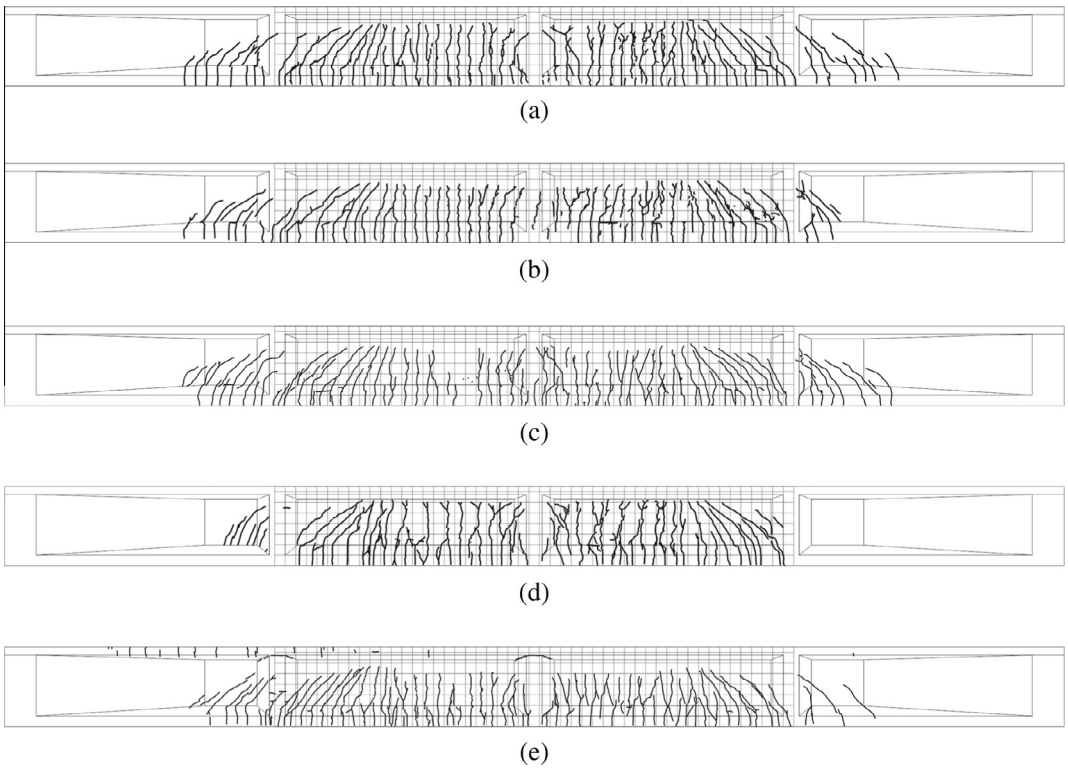

Fig. 6. Crack patterns after the test: (a) NB; (b) NC; (c) ND; (d) HC; and (e) HD.

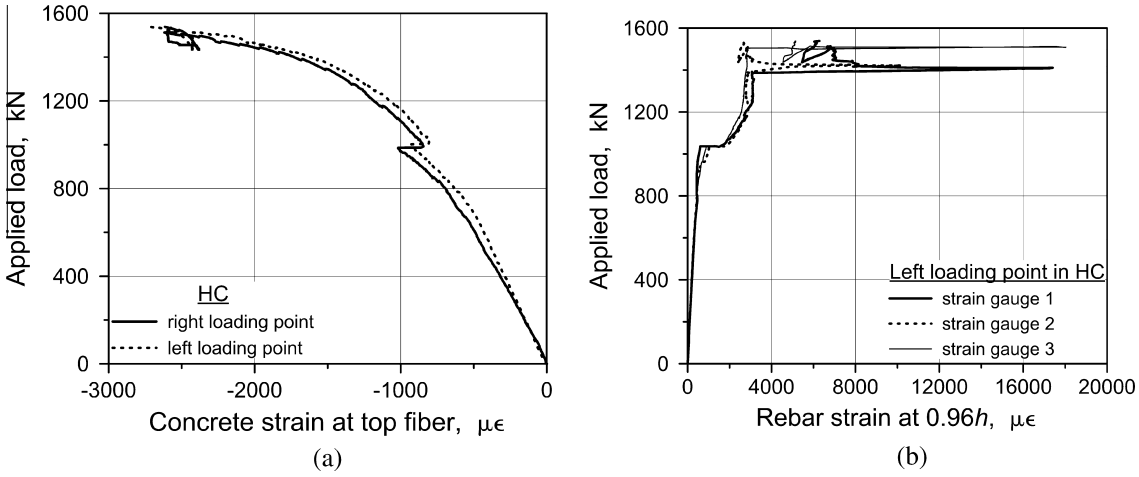

Fig. 7. Measured strains at the left loading point in the specimen HC: (a) concrete strain at top fiber; and (b) rebar strain at 0.96 h.

prestressing steel, respectively, and ω and ω' are the tension and compression rebar indexes, respectively. Note that Eq. (4) is available when the effective prestress f_{se} is larger than half the nominal tensile strength of the strand. Eq. (4) was derived by Mattock [1] from the test results of the prestressed concrete beams with stress-relieved Grade 1860 strands. Therefore, it is required to investigate whether Eq. (4) is applicable even for PSC members with high-strength strands.

For the ND and HD specimens, Fig. 11 shows the stress variation in the strand throughout the test, which was evaluated from the tension strain measured by the LVDTs on the level of the strand at a distance of 1.5 m from the center of the specimens. In the figure, the vertical dotted line represents the stress in the strands estimated by Eq. (4), $f_{ps,ACI}$, and the horizontal solid line corresponds to the nominal flexural strength. The contribution of the deformed rebars to the tensile force on the section was ignored in the calculation of Eq. (4) since the effect of the deformed rebars on $f_{ps,ACI}$ is negligible because of the area of the deformed rebars much smaller than the area of the strands. As shown in the figure, the measured stress in the strands approached the intersection point predicted by ACI 318. The maximum applied load and the corresponding stress in the strands were slightly smaller than the predictions by ACI 318, which is primarily due to the safety issue during the test; the instruments were removed from the specimens before complete failure of the specimens. Because the concrete at the top of the specimens exhibited large compressive

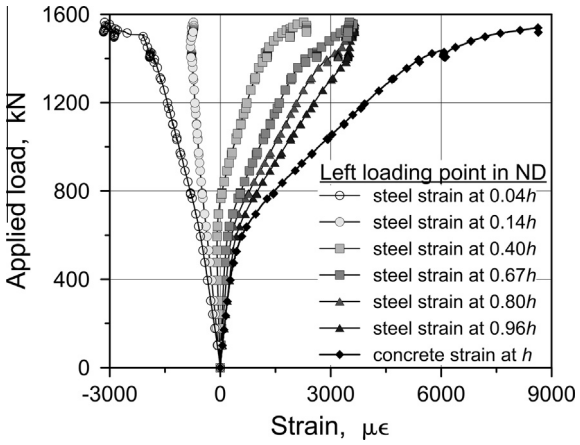

Fig. 8. Measured strains at the left loading point in the specimen ND.

strains close to 0.003, as presented in Fig. 7(a), it can be inferred that the test results at the end of the test was close to the actual flexural failure. Fig. 11 also depicts the analytical results with the solid lines. Multi-layered sectional analysis [17] was employed, which divided a section into multiple layers and calculated curvatures and depths of neutral axis satisfying the compatibility and force equilibrium on the section. Thorenfeldt et al.'s model [18] and elastic-brittle failure model were employed for concrete under compressive and tensile behaviors, respectively. Bi-linear model with the yield strength of 400 MPa and elastic modulus of 200,000 MPa was used for reinforcing steel bars. For the strands, the actual stress–strain relationships in Fig. 1 were used. The analytical results agreed well with the measured stresses in the strands as well as the prediction by ACI 318. Therefore, it can be concluded that the current provisions with Eq. (4) in the ACI 318 code can also be applied to evaluate the flexural strength of PSC beams with high-strength strands.

4.2. Ductile behavior at ultimate failure

In ACI 318 [15], the ductile section with a high net tensile strain has the advantage of a high strength reduction factor because the strength reduction factor is given as a function of net tensile strain; for a net tensile strain larger than 0.005, which is considered as a tension-controlled section, 0.9 can be used for the strength reduction factor. Fig. 12 presents that the net tensile strain at the height of the strands in the ND specimen. The average strain measured at the height of the centroid of the strands was 0.0068, which exceeds the current tension-controlled strain limit of 0.005. The total strain in the strands was estimated 0.014, which was obtained by adding the strain measured at the end of prestressing, i.e., a microstrain of 7538, to the average strain, which exceeded the yield strain of 0.013 determined using the 0.2% offset method [19]. Therefore, it can be concluded that the specimens with high-strength strands exhibited ductile behavior that complies with the ACI 318 provision.

4.3. Crack width

In ACI 318, the equation for the spacing of the reinforcements has an implicit permissible crack width of 0.44 mm for reinforced concrete members [20,21]. For PSC members, the spacing of the reinforcements is required to be two-thirds that of RC members, which reduces the implicit permissible crack width to approximately 0.29 mm ($\approx 0.44 \times 2/3$). However, in Eurocode 2 [16], the crack width must be less than the specified maximum crack width, which is 0.4 and 0.2 mm for RC and PSC members under X0 and XC1 exposure classes, respectively. Fig. 13 shows the measured crack widths within the pure bending region of the ND specimen. In the figure, the permissible crack widths by the ACI 318 code and Eurocode 2 and the full service load are also noted. Note that the crack widths were measured at four locations: 630 and 2098 mm from the center of the specimen to the right and 950 and 2390 mm to the left. At the full service load, the measured maximum crack width was 0.345 mm. Although this value slightly exceeded the permissible crack widths of ACI 318 code, the maximum crack width can easily be controlled with deformed rebars.

Another limitation for crack control in ACI 318 is the stress in the reinforcement closest to the tension face under the service load. The reinforcing steel bar has the limitation of $2/3f_y$, and the stress in the prestressing steel after decompression Δf_{ps} should not exceed 250 MPa. Fig. 14 shows the measured Δf_{ps} and f_s of the ND and HD specimens. The minus stress in the reinforcing steel bars resulted from the compressive stress induced by prestressing. The stress in the prestressing strands was lowered by the same amount to the compressive strain in the reinforcing steel bars at the same section. When Δf_{ps} reaches zero, it can be said that the section is decompressed. At the full service load, several of the measured Δf_{ps} and f_s values exceeded the limitation. The reinforcing

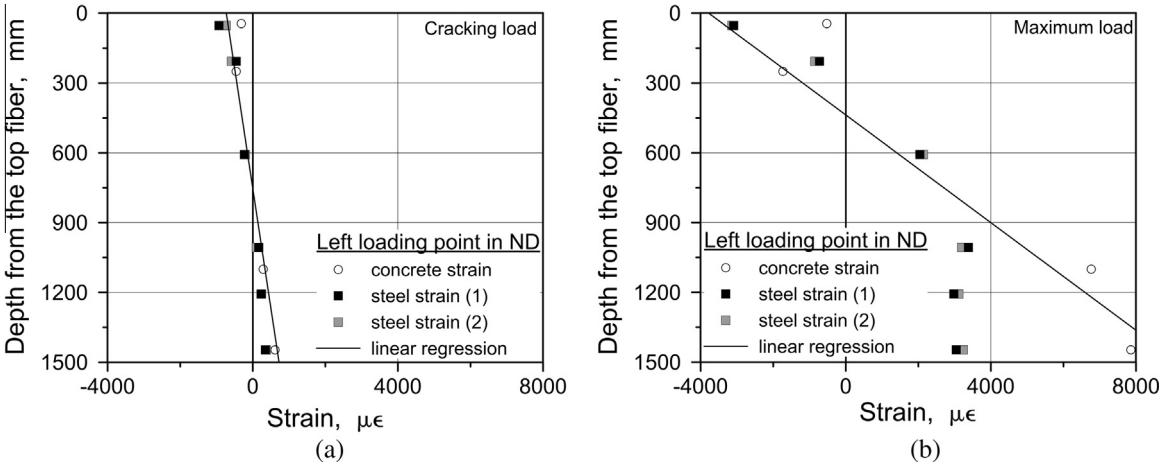

Fig. 9. Strain distribution along the depth in the specimen ND: (a) at cracking load; and (b) at maximum load.

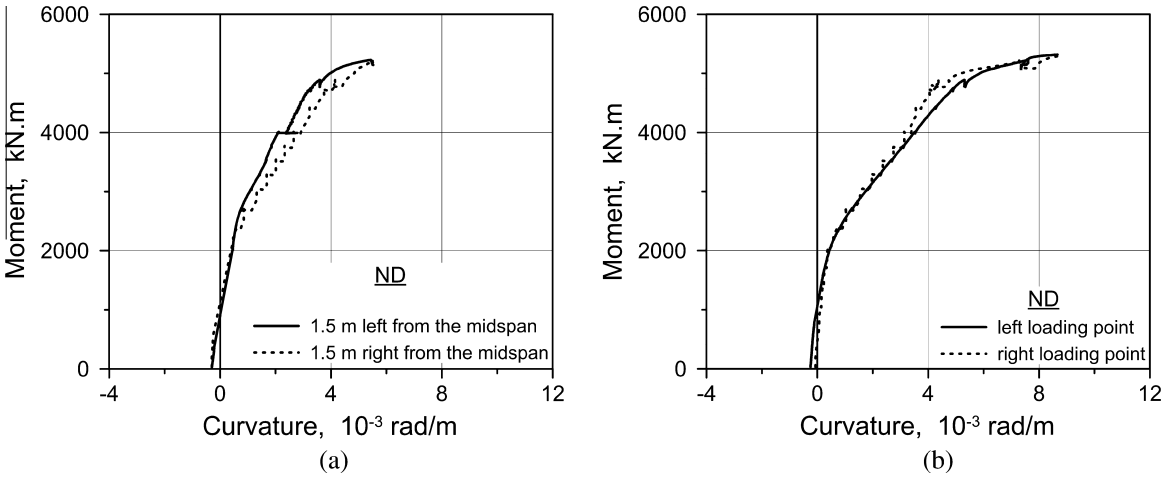

Fig. 10. Moment–curvature response: (a) at the sections 1.5 m from the center; and (b) at the loading points in the specimen ND.

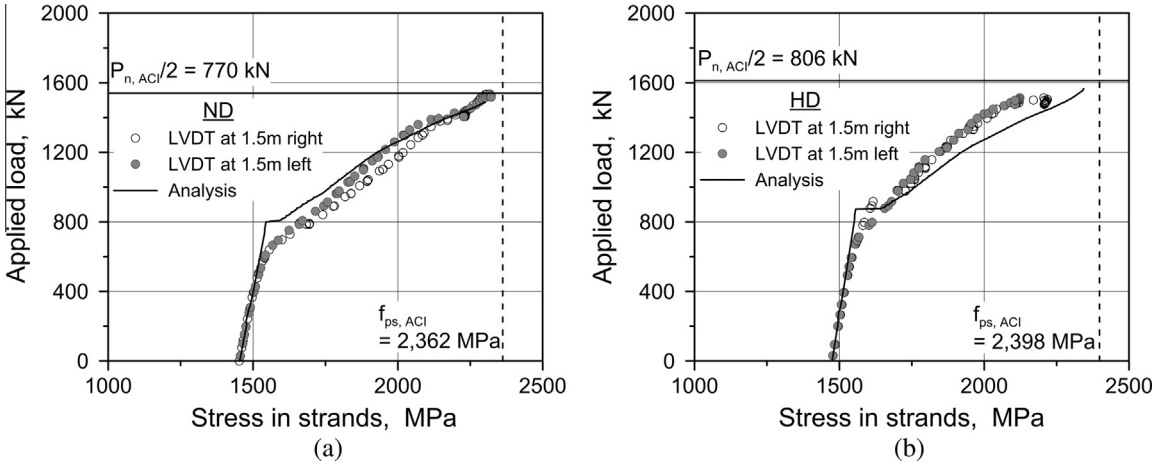

Fig. 11. Measured stresses in strands at the sections 1.5 m from the center: (a) ND; and (b) HD.

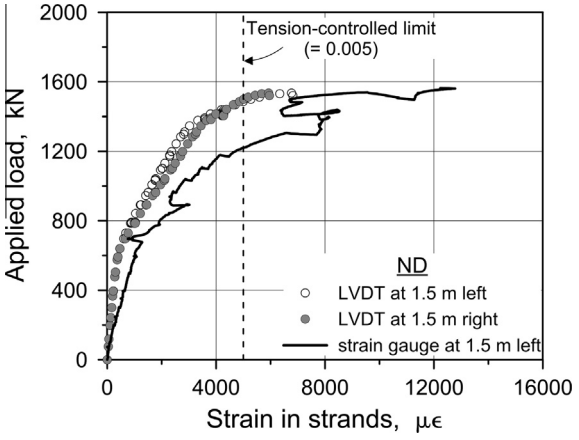

Fig. 12. Measured strain in strands at the sections 1.5 m from the center in the specimen ND.

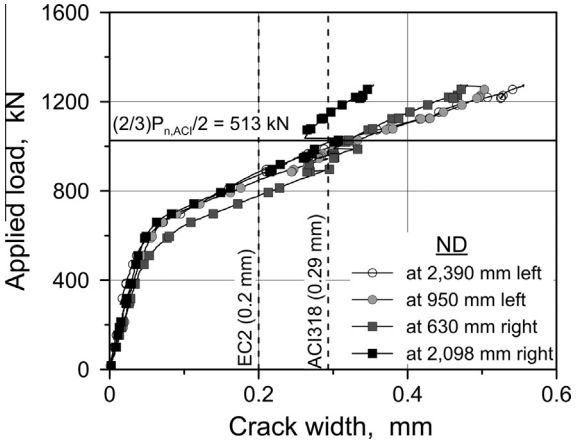

Fig. 13. Measured crack widths in the pure bending region in the specimen ND.

steel bars that exhibited the largest stress were likely to be located at the cracked sections in the previous loading stage. Excluding those steel bars, the value of Δf_{ps} and f_s ranged between 154 MPa and 304 MPa, and the average stress was 227 MPa. Most of the measurements did not exceed the limitation of $2/3f_y$ (267 MPa); however, several measurements did not satisfy the requirement of the current code similarly to the crack width. Therefore, further study is required to determine the limitations on Δf_{ps} and f_s when considering the tensile strength of the strands.

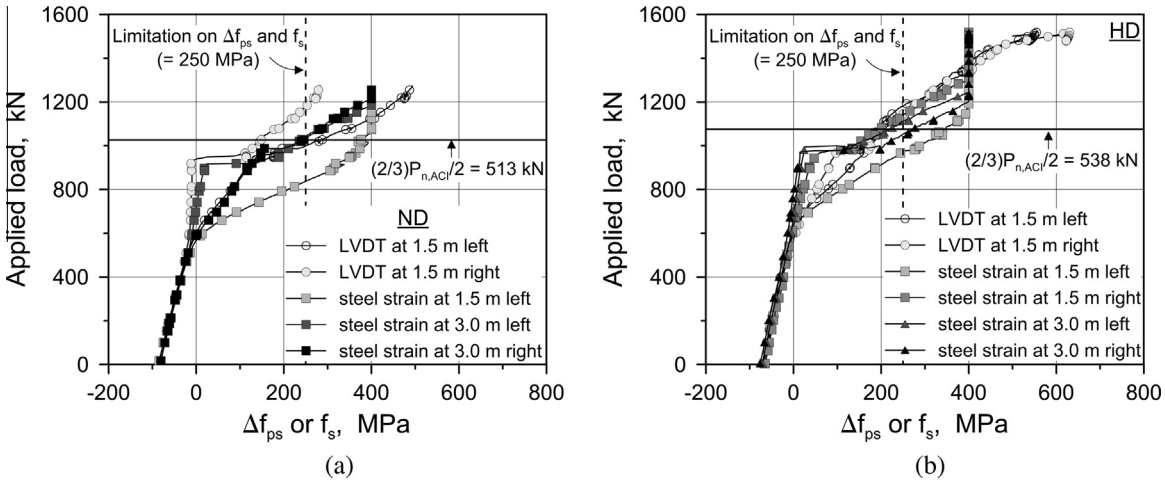

Fig. 14. Measured stresses in strands and deformed rebars: (a) ND; and (b) HD.

5. Conclusions

The following conclusions can be drawn from this study, which encompassed experimental and numerical investigations of PSC girders with high-strength strands, as well as code implications for their use.

1. The specimens exhibited ductile flexural behavior regardless of the tensile strength of the strands. From the net tensile strains measured in the strands, the specimens were categorized into a tension-controlled section defined in ACI 318.
2. The flexural behaviors of the specimens were estimated well by the current ACI 318 code. The nominal flexural strength and the corresponding stress in the strands predicted by the current code gave close estimations to the test results, even for the specimen with high strength concrete and high strength strands.
3. The crack patterns and crack spacing were similar for all the specimens regardless of the tensile strength of the prestressing strands if deformed rebars were identically provided in the tensile area of the concrete section.
4. The maximum crack width in the specimen with high-strength strands under the full service load slightly exceeded the permissible value of ACI 318; however, this can easily be controlled with an appropriate arrangement of deformed bars.
5. Several stress values in the high-strength strands and deformed rebars under the full service load slightly exceeded the permissible values of ACI 318 code. Further study is required to determine the limitations on Δf_{ps} and f_s when considering the tensile strength of the strands.

Acknowledgements

This research was supported by Institute of Construction and Environmental Engineering at Seoul National University. The authors wish to express their gratitude for the support.

References

[1] Mattock AH. Modification of ACI code equation for stress in bonded prestressed reinforcement at flexural ultimate. ACI J 1984(July–August):331–9.
[2] Devalapura RK, Tadros MK. Stress-strain modeling of 270 ksi low-relaxation prestressing strands. PCI J 1992;37(2):100–5.
[3] Roller JJ, Martin BT, Russell HG, Bruce RN. Performance of prestressed high strength concrete bridge girders. PCI J 1993;38(3):34–45.
[4] Ng CK, Tan KH. Flexural behaviour of externally prestressed beams. Part I: Analytical model. Eng Struct 2006;28:609–21.
[5] Ng CK, Tan KH. Flexural behaviour of externally prestressed beams. Part II: Experimental Investigation. Eng Struct 2006;28:622–33.
[6] Kaewunruen S, Remennikov AM. Progressive failure of prestressed concrete sleepers under multiple high-intensity impact loads. Eng Struct 2009;31:2460–73.
[7] Yuan A, Dai H, Sun D, Cai J. Behaviors of segmental concrete box beams with internal tendons and external tendons under bending. Eng Struct 2013;48:623–34.
[8] Vázquez-Herrero C, Martínez-Lage I, Martínez-Abella F. Transfer length in pretensioned prestressed concrete structures composed of high performance lightweight and normal-weight concrete. Eng Struct 2013;56:983–92.
[9] Kim YH, Hueste MB, Trejo D. Flexural behavior of high-early-strength self-consolidating concrete pretensioned bridge girders: experimental evaluation. ASCE J Bridge Eng 2015;20(2):04014064.
[10] Yamada M. Recent topics on prestressing steel. Concr J 2009;47(11):3–8.
[11] Hill AT. Material properties of the Grade 300 and Grade 270 prestressing strands and their impact on the design of bridges [Master's thesis]. Virginia Polytechnic Institute and State University; 2006.
[12] Carroll JC. Grade 300 prestressing strand and the effect of vertical casting position [PhD Thesis]. Virginia Polytechnic Institute and State University; 2009.
[13] KS D 7002. Uncoated stress-relieved steel wires and strands for prestressed concrete. Seoul, South Korea: Korean Agency for Technology and Standards; 2011.
[14] Korean Society of Civil Engineering. Korean Highway and Bridge Design Code. Seoul, South Korea; 2008.
[15] ACI Committee 318. Building code requirements for structural concrete (ACI 318-11). Farmington Hills (MI): American Concrete Institute; 2011.
[16] European Committee for Standardization. Eurocode2: design of concrete structures. Part 1–1: General rules and rules for buildings; 2004.
[17] Bentz EC. Sectional analysis of reinforced concrete members [PhD Thesis]. Toronto, ON, Canada: Department of Civil Engineering, University of Toronto; 2000.
[18] Thorenfeldt E, Tomaszewicz A, Jensen JJ. Mechanical properties of high strength concrete and application to design. In: Proceedings of the symposium: utilization of high-strength concrete; 1987. p. 149–59.
[19] ASTM A 370-14. Standard test methods and definitions for mechanical testing of steel products. West Conshohocken (PA): ASTM International; 2014.
[20] ACI Committee 224. Control of cracking in concrete structures (ACI 224R-01). Farmington Hills (MI): American Concrete Institute; 2001.
[21] Ospina CE, Bakis CE. Indirect flexural crack control of concrete beams and one-way slabs reinforced with FRP bars. In: The 8th international symposium on fiber reinforced polymer reinforcement for concrete structures (FRPRCS-8). Patras, Greece; 2007. p. 16–8.